J Biomol NMR (2007) 37:245–255
DOI 10.1007/s10858-006-9126-6

ARTICLE

Improved magnetization alignment schemes for spin-lock relaxation experiments

D. Flemming Hansen · Lewis E. Kay

Received: 27 October 2006 / Accepted: 27 November 2006 / Published online: 20 February 2007

Abstract A pair of pulse schemes that spin-lock magnetization efficiently are presented. The design of the sequences benefited from a particularly simple relation that is derived describing to first order the evolution of any magnetization component due to the application of an off-resonance 90° pulse. The sequences are shown theoretically and experimentally to significantly outperform the 90°-delay-90° element that is often used in current applications. It is shown that alignment of magnetization to within 1° of the effective field can be obtained over a bandwidth extending between $[-\omega_{SL}, \omega_{SL}]$, where ω_{SL} is the strength of the spin-lock field using a simple scheme that is an order of magnitude shorter than an adiabatic pulse that might also be used for a similar purpose.

Keywords Magnetization alignment · Spin-lock · $R_{1\rho}$ relaxation · Off-resonance 90° pulse

Introduction

It has long been known that ^{13}C and ^{15}N spin relaxation experiments can provide useful information about protein dynamics (Allerhand et al. 1971; Gust et al. 1975; Richarz et al. 1980; Henry et al. 1986). However, the widespread utility of such experiments had to await the development of heteronuclear two-dimensional NMR methods (Ernst et al. 1987) that provide access to motion on a per residue basis and that increase the sensitivity of such measurements by probing the relaxation properties of the heteroatom through a series of 2D ^{1}H-detected correlation spectra (Nirmala and Wagner 1988; Kay et al. 1989b). Over the past two decades, since the establishment of the initial experiments, a large number of methods have been presented for quantifying motion over a wide spectrum of time-scales (Dayie et al. 1996; Palmer et al. 1996; Ishima and Torchia 2000; Palmer et al. 2005). Among the most important of experiments are those that measure heteroatom spin–spin relaxation properties that form the basis for the extraction of order parameters that provide information on the amplitude of dynamics at a given site in the molecule. Included in this set of experiments are those that measure $R_{1\rho}$ values where the decay of magnetization aligned along an effective magnetic field is monitored (Deverell et al. 1970; Peng and Wagner 1992). These experiments are also of interest in the study of ms–μs time-scale processes that are quantified through the dependence of $R_{1\rho}$ on the effective field (Palmer et al. 2001).

A prerequisite for the extraction of accurate $R_{1\rho}$ values is to ensure that magnetization is aligned properly along the effective magnetic field prior to the spin-lock period. During the spin-lock interval the effective magnetic field experienced by a nuclear spin in the rotating frame is the vector-sum of two orthogonal components, that are in turn proportional

Electronic supplementary material The online version of this article (doi:10.1007/s10858-006-9126-6) contains supplementary material, which is available to authorized users.

D. F. Hansen · L. E. Kay (✉)
Departments of Medical Genetics, Biochemistry and Chemistry, The University of Toronto, 1 King's College Circle, Toronto, ON, Canada M5S 1A8
e-mail: kay@pound.med.utoronto.ca

to the offset from the radio frequency (RF) carrier in the rotating frame, $\vec{\Omega}$, and to the field strength of the continuous wave RF field used for the spin-lock, $\vec{\omega}_{SL}$, so that $\vec{\omega}_{eff,SL} = \vec{\Omega} + \vec{\omega}_{SL}$. Of primary interest is the component of the nuclear magnetization that is parallel to the effective field that relaxes due to $R_{1\rho}$ processes, while the component of the magnetization that is orthogonal to the effective magnetic field is dephased during the spin-lock period from in-homogeneities in the spin-lock field and $R_{2\rho}$ processes. Components orthogonal to the effective field that are present at the beginning of the spin-lock period can lead to non-exponential decay of signal intensity for initial time points that, in turn, hamper the extraction of reliable $R_{1\rho}$ relaxation rates.

With this problem in mind pulse schemes have been developed for placing magnetization components along their effective fields prior to the spin-lock interval in $R_{1\rho}$ relaxation experiments. These make use of adiabatic sweep techniques (Mulder et al. 1998) or alternatively pulse trains (Griesinger and Ernst 1987; Yamazaki et al. 1994; Akke and Palmer 1996) that are based on a combination of high power RF pulses and delays. The alignment obtained with the adiabatic sweep technique is superior to that generated with the second approach, however, the required duration of the adiabatic pulse is often considerably longer (several ms) (Mulder et al. 1998; Palmer and Massi 2006) than for the method that uses delays/high power pulses, leading potentially to larger sensitivity losses due to relaxation. In addition, in cases where ms–μs dynamics are of interest, exchange during the (lengthy) adiabatic sweep interval can potentially lead to initial magnetization conditions that do not reflect the equilibrium distribution of spin states. Finally, because the relaxation properties during the adiabatic sweep must be accounted for, at least two different spin-lock relaxation times points must be obtained for each effective field or a correction scheme must be employed if only a single point is recorded (Korzhnev et al. 2003). With these issues in mind it is of considerable interest to develop new alignment schemes that utilize RF pulses/delays that offer improvements in alignment over existing pulse/delay methods and that approach the adiabatic sweep methods in terms of degree of alignment, but that can be executed in much shorter intervals. In what follows we present the theory to understand how such sequences can be constructed, along with a number of elements that offer significant advances over approaches that are currently available.

Results and discussion

The off-resonance 90° pulse

Prior to a discussion of new pulse/delay alignment schemes we first consider a few basic rules that describe in a very simple way how an off-resonance 90° pulse affects magnetization. Although the formalism for the description of off-resonance effects is well known (Ernst et al. 1987) and off-resonance excitation is well understood (Ernst et al. 1987; Marion and Bax 1988) a review is in order because the relations that we will derive will become very useful when we consider more complex pulse schemes. For an isolated spin an off-resonance 90° RF pulse applied with x-phase causes rotation of magnetization according to

$$\hat{R}_{\frac{\pi}{2}x} = \hat{R}_y\left(\theta - \frac{\pi}{2}\right)\hat{R}_x\left(\frac{\pi}{2}\sqrt{1+\frac{\Omega^2}{\omega_1^2}}\right)\hat{R}_y\left(\frac{\pi}{2} - \theta\right), \quad (1)$$

where $\hat{R}_x(\alpha)$ and $\hat{R}_y(\alpha)$ are the conventional matrices for active rotations about the x- and y-axis by α radians, respectively, $\vec{\Omega}$ is the offset of the spin from the RF carrier (rad/s), $\vec{\omega}_1$ is the field of the RF pulse (rad/s), and θ is the angle between the z-axis and $\vec{\omega}_{eff,1} = \vec{\omega}_1 + \vec{\Omega}$, i.e. $\tan(\theta) = \omega_1/\Omega$. More specifically, $\hat{R}_{\frac{\pi}{2}x}$ describes the rotation of the magnetization about the axis $\vec{\omega}_{eff,1}/\|\vec{\omega}_{eff,1}\|$ by $\pi\omega_{eff,1}/2\omega_1$. The rotation generated by an off-resonance 90° RF pulse with y-phase is described in a similar manner by three consecutive rotations.

Equation (1) can be recast in terms of the standard product operator formalism (Sørensen et al. 1983). With $\boldsymbol{\sigma}_{init}$ the initial density operator of the spin system prior to the application of the pulse and $\boldsymbol{\sigma}_{final}$ the density operator immediately after the pulse, $\boldsymbol{\sigma}_{final} = \mathbf{U}\boldsymbol{\sigma}_{init}\mathbf{U}^{-1}$, where $\mathbf{U}$ is the propagator

$$\mathbf{U} = \exp(i\varphi\mathbf{I}_y)\exp\left(-i\frac{\pi}{2}\sqrt{1+\frac{\Omega^2}{\omega_1^2}}\mathbf{I}_x\right)\exp(-i\varphi\mathbf{I}_y), \quad (2)$$

and $\varphi = \pi/2–\theta$ is the angle between the x-axis and $\vec{\omega}_{eff,1}$.

Application to longitudinal magnetization

The commutation relationship, $[\mathbf{I}_x, \mathbf{I}_y] = i\,\mathbf{I}_z$, implies that

$$\exp\left(i\frac{\pi}{2}\mathbf{I}_x\right)\exp(-i\varphi\mathbf{I}_z)\exp\left(-i\frac{\pi}{2}\mathbf{I}_x\right) = \exp(-i\varphi\mathbf{I}_y) \quad (3)$$

so that from Eq. (2) the propagator for the application of an off-resonance 90° x-pulse can be written as

$$\begin{aligned}\mathbf{U} = &\exp\left(i\varphi\mathbf{I}_y\right)\exp\left(-i\frac{\pi}{2}\sqrt{1+\frac{\Omega^2}{\omega_1^2}}\mathbf{I}_x\right)\exp\left(i\frac{\pi}{2}\mathbf{I}_x\right)\\ &\times\exp\left(-i\varphi\mathbf{I}_z\right)\exp\left(-i\frac{\pi}{2}\mathbf{I}_x\right).\end{aligned} \tag{4}$$

In what follows we assume that $\Omega << \omega_1$, which implies that $\varphi \approx \tan(\varphi) = \Omega/\omega_1$. Thus, $\sqrt{1+\Omega^2/\omega_1^2} \approx 1+\Omega^2/2\omega_1^2 \approx 1$, and the propagator of Eq. (4) reduces to

$$\mathbf{U} \approx \exp\left(i\varphi\mathbf{I}_y\right)\exp\left(-i\varphi\mathbf{I}_z\right)\exp\left(-i\frac{\pi}{2}\mathbf{I}_x\right). \tag{5}$$

The first exponential (from the right) in Eq. (5) describes an ideal 90° x-pulse, the second corresponds to evolution for a period of length $1/\omega_1$ and the last term, $\exp(i\varphi\mathbf{I}_y)$, describes a clockwise rotation about the y-axis in the amount φ; this rotation can be neglected since for $\varphi << 1$ the vast majority of the magnetization is aligned along the y-axis when the y-rotation is applied. In conclusion, the rotation of equilibrium z magnetization by the off-resonance 90° x-pulse is described, to a good approximation, by

$$\begin{aligned}\mathbf{I}_z &\xrightarrow{\frac{\pi}{2}\mathbf{I}_x} -\mathbf{I}_y \xrightarrow{\Omega/\omega_1\mathbf{I}_z} -\mathbf{I}_y\cos(\Omega/\omega_1)+\mathbf{I}_x\sin(\Omega/\omega_1)\\ &\xrightarrow{\Omega/\omega_1\mathbf{I}_y} -\mathbf{I}_y\cos(\Omega/\omega_1)\\ &\quad+\mathbf{I}_x\sin(\Omega/\omega_1)\cos(\Omega/\omega_1)+\mathbf{I}_z\sin^2(\Omega/\omega_1)\\ &\approx -\mathbf{I}_y\cos(\Omega/\omega_1)+\mathbf{I}_x\sin(\Omega/\omega_1).\end{aligned} \tag{6}$$

The fact that off-resonance effects can be treated in terms of evolution periods has enormous practical importance in the design of pulse sequences. As an example, off-resonance effects cause first order phase distortions in the indirect dimensions of a multi-dimensional NMR spectrum that can be removed easily by taking into account the evolution period that accompanies each 90° pulse (Marion and Bax 1988; Kay et al. 1989a). Finally, it is worth noting that we can write

$$\mathbf{U} \approx \exp\left(-i\frac{\Omega}{\omega_1}\mathbf{I}_z\right)\exp\left(-i\frac{\pi}{2}\mathbf{I}_x\right)\exp\left(-i\frac{\Omega}{\omega_1}\mathbf{I}_z\right) \tag{7}$$

since $[\exp(-i(\Omega/\omega_1)\mathbf{I}_z), \mathbf{I}_z] = 0$; the reason for doing this will be come clear shortly.

Application to transverse magnetization

Let us first consider the off-resonance effects of a 90° x pulse applied to magnetization along the y-axis. We begin by taking the propagator, $\mathbf{U}$, for the off-resonance 90° x pulse, Eq. (2), and rewriting it as

$$\begin{aligned}\mathbf{U} &= \exp\left(i\varphi\mathbf{I}_y\right)\exp\left(-i\frac{\pi}{2}\sqrt{1+\frac{\Omega^2}{\omega_1^2}}\mathbf{I}_x\right)\exp\left(-i\varphi\mathbf{I}_y\right)\\ &= \exp\left(-i\frac{\pi}{2}\mathbf{I}_x\right)\exp\left(-i\varphi\mathbf{I}_z\right)\\ &\quad\times\exp\left(i\frac{\pi}{2}\mathbf{I}_x\right)\exp\left(-i\frac{\pi}{2}\sqrt{1+\frac{\Omega^2}{\omega_1^2}}\mathbf{I}_x\right)\exp\left(-i\varphi\mathbf{I}_y\right)\\ &\approx \exp\left(-i\frac{\pi}{2}\mathbf{I}_x\right)\exp\left(-i\varphi\mathbf{I}_z\right)\exp\left(-i\varphi\mathbf{I}_y\right).\end{aligned} \tag{8}$$

The first exponential in Eq. (8) has no effect when applied to magnetization aligned along the y-axis, because $[\mathbf{I}_y, \mathbf{I}_y] = 0$. Thus, so long as $\Omega << \omega_1$, the off-resonance 90° x-pulse can be treated as an evolution period of length $1/\omega_1$ followed by an ideal 90° x-pulse

$$\begin{aligned}\mathbf{I}_y &\xrightarrow{\Omega/\omega_1\mathbf{I}_y} \mathbf{I}_y \xrightarrow{\Omega/\omega_1\mathbf{I}_z} \mathbf{I}_y\cos(\Omega/\omega_1)-\mathbf{I}_x\sin(\Omega/\omega_1)\\ &\xrightarrow{\frac{\pi}{2}\mathbf{I}_x} \mathbf{I}_z\cos(\Omega/\omega_1)-\mathbf{I}_x\sin(\Omega/\omega_1).\end{aligned} \tag{9}$$

It is worth noting that for $\Omega << \omega_1$ the component of magnetization along the z-axis is very much larger than the x-component and it follows, therefore, that a subsequent rotation about the z-axis (by φ) changes the final magnetization state very little. Thus, the rotation propagator $\mathbf{U}$, Eq. (8), is also very well approximated by Eq. (7).

Finally, this formalism can also be used to understand how an off-resonance 90° x-pulse affects x-magnetization. As above, the propagator is rewritten in order to better understand the induced rotation

$$\begin{aligned}\mathbf{U} &= \exp\left(i\varphi\mathbf{I}_y\right)\exp\left(-i\frac{\pi}{2}\sqrt{1+\frac{\Omega^2}{\omega_1^2}}\mathbf{I}_x\right)\\ &\quad\times\exp\left(i\frac{\pi}{2}\mathbf{I}_x\right)\exp\left(-i\varphi\mathbf{I}_z\right)\exp\left(-i\frac{\pi}{2}\mathbf{I}_x\right)\\ &\approx \exp\left(i\frac{\pi}{2}\mathbf{I}_x\right)\exp\left(i\varphi\mathbf{I}_z\right)\exp\left(-i\frac{\pi}{2}\mathbf{I}_x\right)\\ &\quad\times\exp\left(-i\varphi\mathbf{I}_z\right)\exp\left(-i\frac{\pi}{2}\mathbf{I}_x\right),\end{aligned} \tag{10}$$

and $\mathbf{U}\mathbf{I}_x\mathbf{U}^{-1}$ gives

$$\begin{aligned}\mathbf{I}_x &\xrightarrow{\frac{\pi}{2}\mathbf{I}_x} \mathbf{I}_x \xrightarrow{\varphi\mathbf{I}_z} \mathbf{I}_x\cos(\varphi)+\mathbf{I}_y\sin(\varphi)\\ &\xrightarrow{\frac{\pi}{2}\mathbf{I}_x} \mathbf{I}_x\cos(\varphi)+\mathbf{I}_z\sin(\varphi)\end{aligned} \tag{11}$$

$$\xrightarrow{-\varphi\mathbf{I}_z} \mathbf{I}_x\cos^2(\varphi)-\mathbf{I}_y\cos(\varphi)\sin(\varphi)+\mathbf{I}_z\sin(\varphi) \tag{12}$$

$$\xrightarrow{-\frac{\pi}{2}\mathbf{I}_x} \mathbf{I}_x\cos^2(\varphi)+\mathbf{I}_y\sin(\varphi)+\mathbf{I}_z\cos(\varphi)\sin(\varphi). \tag{13}$$

The first rotation has no effect on x-magnetization, while the subsequent two rotations describe an evolution period of length $1/\omega_1$ followed by an ideal 90° x-pulse. The final pair of exponentials in the second expression of Eq. (10) can be replaced to first order (i.e, for $\Omega << \omega_1$) by an additional evolution period of duration $1/\omega_1$. That this is the case can be seen by starting from the final density term of Eq. (11), evolving for $1/\omega_1$ to produce $\mathbf{I}_x \cos^2(\varphi) + \mathbf{I}_y \cos(\varphi)\sin(\varphi) + \mathbf{I}_z \sin(\varphi)$, and noting that $\cos(\varphi)\sin(\varphi) \approx \sin(\varphi)$. Once again we see that the propagator of Eq. (7) provides an accurate description (to first order) for the evolution of magnetization (in this case the x-component) during an off-resonance 90° x-pulse.

Thus, the application of an off-resonance 90° x-pulse to any of the Cartesian basis vectors of an isolated spin system can be treated as (1) an evolution period of length $1/\omega_1$ followed by (2) an ideal 90° pulse and finally by (3) a second evolution period of length $1/\omega_1$, Eq. (7). In a similar manner Eq. (7) can be modified to account for an off-resonance 90° y-pulse by replacing $\mathbf{I}_x$ with $\mathbf{I}_y$. The validity of this approximation is demonstrated in Fig. 1, where Eq. (7) is used to evaluate $\mathbf{U}\mathbf{I}_x\mathbf{U}^{-1}$ and the result compared with the case where the genuine propagator, Eq. (2), is employed. As seen from Fig. 1, the approximate propagator describes quite well the induced rotation of magnetization in situations that are normally encountered in solution state NMR studies when high power pulses are applied.

Pulse schemes for magnetization alignment

The general approximation that an off-resonance 90° pulse can be treated as an ideal pulse flanked by two evolution periods of length $1/\omega_1$ allows us to optimize pulse schemes for alignment of magnetization along an effective field. In what follows below we first briefly review an existing scheme to highlight its limitations and then proceed with new approaches that offer significant improvements.

For a spin with a small offset from the RF carrier, $-0.4\omega_{SL} < \Omega < 0.4\omega_{SL}$, the pulse-scheme (Yamazaki et al. 1994; Akke and Palmer 1996)

$$90^\circ_{\pm y} - \chi - 90^\circ_x, \tag{14}$$

where $\chi = 1/\omega_{SL} - 2/\omega_1$ rotates to a reasonable approximation magnetization from the $+z$-axis to the effective spin-lock field, $\vec{\omega}_{\mathrm{eff,SL}} = \vec{\omega}_{SL} + \vec{\Omega}$ (to within several degrees, see Fig. 2 below). Here, the phase of the initial 90° pulse is inverted together with the receiver. The total rotation of the magnetization caused by this pulse scheme is described by the three consecutive unitary rotations, $\hat{R}_{\frac{\pi}{2}x}\hat{R}_z(\chi\Omega)\hat{R}_{\pm\frac{\pi}{2}y}$, where the χ delay is treated as a pure z rotation. Thus, the propagator for the alignment scheme can, to a first order approximation and according to the discussion above, be written as

$$\begin{aligned}\mathbf{U} \approx & \exp\left(\frac{-i\Omega}{\omega_1}\mathbf{I}_z\right)\exp\left(\frac{-\pi i}{2}\mathbf{I}_x\right)\exp\left(\frac{-i\Omega}{\omega_1}\mathbf{I}_z\right) \\ & \times \exp\left(-i\left(\frac{\Omega}{\omega_{SL}} - \frac{2\Omega}{\omega_1}\right)\mathbf{I}_z\right) \\ & \times \exp\left(\frac{-i\Omega}{\omega_1}\mathbf{I}_z\right)\exp\left(\frac{\mp\pi i}{2}\mathbf{I}_y\right)\exp\left(\frac{-i\Omega}{\omega_1}\mathbf{I}_z\right).\end{aligned} \tag{15}$$

The evolution periods following and preceding the 90° y and 90° x-pulses, respectively, that account for off-resonance effects, are included in the χ delay by subtracting $2/\omega_1$, while the initial evolution period [first exponential in Eq. (15)] is neglected since the pulse scheme is applied to equilibrium z magnetization. Thus, we can write

$$\mathbf{U} = \exp\left(\frac{-i\Omega}{\omega_1}\mathbf{I}_z\right)\exp\left(\frac{-\pi i}{2}\mathbf{I}_x\right)\exp\left(\frac{-i\Omega}{\omega_{SL}}\mathbf{I}_z\right)\exp\left(\frac{\mp\pi i}{2}\mathbf{I}_y\right) \tag{16}$$

so that magnetization evolves according to

$$\begin{aligned}\mathbf{I}_z \xrightarrow{\pm\frac{\pi}{2}\mathbf{I}_y} & \pm\mathbf{I}_x \xrightarrow{\frac{i\Omega}{\omega_{SL}}\mathbf{I}_z} \pm\mathbf{I}_x\cos(\Omega/\omega_{SL}) \pm \mathbf{I}_y\sin(\Omega/\omega_{SL}) \\ & \xrightarrow{\frac{\pi}{2}\mathbf{I}_x} \pm\mathbf{I}_x\cos(\Omega/\omega_{SL}) \pm \mathbf{I}_z\sin(\Omega/\omega_{SL}) \\ & \xrightarrow{\frac{i\Omega}{\omega_1}\mathbf{I}_z} \pm\mathbf{I}_x\cos(\Omega/\omega_{SL})\cos(\Omega/\omega_1) \\ & \quad \pm \mathbf{I}_y\cos(\Omega/\omega_{SL})\sin(\Omega/\omega_1) \pm \mathbf{I}_z\sin(\Omega/\omega_{SL})\end{aligned} \tag{17}$$

and

$$\begin{aligned}\frac{M_z}{M_x} &\approx \tan\left(\frac{\Omega}{\omega_{SL}}\right) \approx \frac{\Omega}{\omega_{SL}} + \frac{1}{3}\frac{\Omega^3}{\omega_{SL}^3} \\ \frac{M_y}{M_x} &\approx \tan\left(\frac{\Omega}{\omega_1}\right) \approx \frac{\Omega}{\omega_1}.\end{aligned} \tag{18}$$

It should be noted that for perfect alignment along the effective field $M_z/M_x = \Omega/\omega_{SL}$ and $M_y/M_x = 0$. Equation (18) establishes that for nuclei with small offsets from the RF carrier ($\Omega << \omega_1$ and $\Omega < 0.4\omega_{SL}$) the pulse scheme aligns each magnetization component

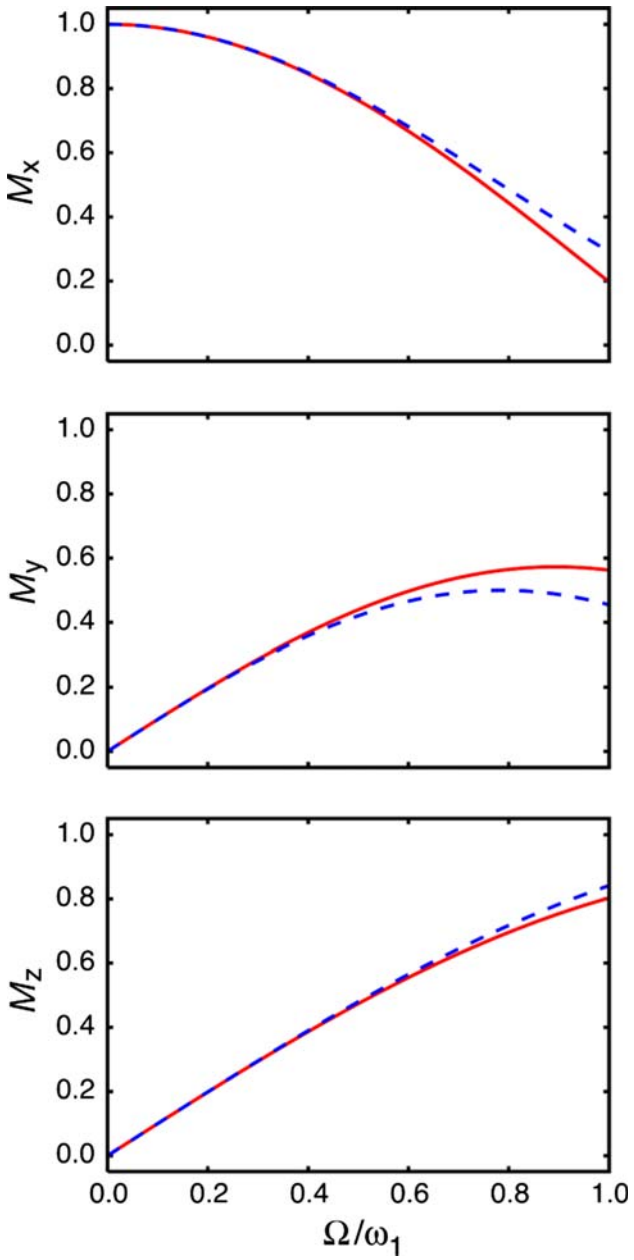

Fig. 1 Magnetization components generated by the application of an off-resonance 90° x-pulse to $\mathbf{I}_x$. The red, continuous line derives from simulations that consider the full propagator, Eq. (2), while the dashed blue lines are obtained using the propagator of Eq. (7). It is seen that the approximate equation is valid in the range $\Omega/\omega_1 \leq 0.3$, that holds in many solution NMR applications that use high power pulses

along its effective spin-lock field reasonably well. However, the component of magnetization orthogonal to the effective field and proportional to Ω/ω_1 causes artifacts and a non-exponential decay of magnetization in the $R_{1\rho}$ experiment for spins with larger offsets. This misalignment appears because chemical shift evolution

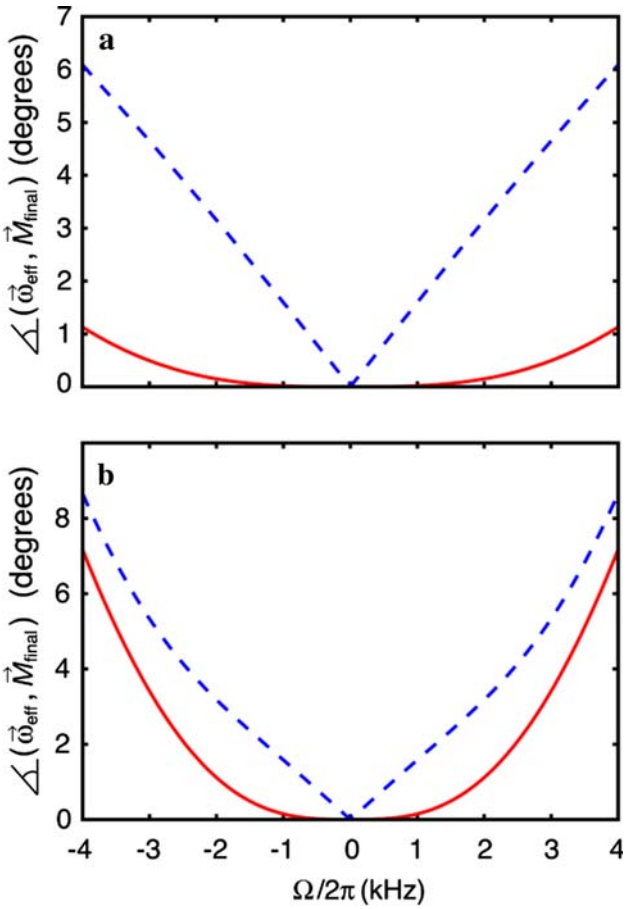

Fig. 2 Alignment of ^{1}H magnetization along the effective magnetic field, $\vec{\omega}_{\rm eff,SL}$, quantified by calculating the angle between $\vec{\omega}_{\rm eff,SL}$ and the magnetization, $\vec{M}_{\rm final}$, that immediately follows application of the alignment schemes of Eqs. (14), (19). The dashed (blue) and continuous (red) lines correspond to the alignment obtained using $90°_{\pm y} - \chi - 90°_{x}$ and $90°_{\pm y} - \chi - 90°_{x} - 180°_{\pm y} - \zeta$, respectively. The field strength used for high power pulses is $\omega_1/2\pi$ = 35.7 kHz, while $\omega_{\rm SL}/2\pi$ = 10 kHz (**a**) and 5 kHz (**b**)

during the final off-resonance 90°_x pulse converts M_x in part to M_y, as detailed in Fig. 1.

Removing artifacts to first order

The pulse scheme of Eq. (14) can be modified so as to remove the misalignment caused by chemical shift evolution during the final 90° pulse

$$90^\circ_{\pm y} - \chi - 90^\circ_x - 180^\circ_{\pm y} - \zeta, \tag{19}$$

where $\zeta = 1/\omega_1$, and the phase cycle $\pm y$ is executed together with an inversion of the receiver. The accuracy of the alignment obtained by the sequence in Eq. (19) can be evaluated by considering a Taylor expansion of the final density operator for spins with an offset smaller

than the spin-lock field strength, $\Omega < \omega_{SL}$. Here, the final density operator is calculated by treating the off-resonance pulses rigorously, Eq. (2), and a Taylor expansion to third order is performed for the three individual Cartesian components

$$\boldsymbol{\sigma}_{\text{final}} = (\mathbf{I}_x\ \mathbf{I}_y\ \mathbf{I}_z)\begin{pmatrix} \mp 1 \pm \frac{1}{2}\frac{\Omega^2}{\omega_{SL}^2} - \left(2+\frac{\pi}{2}\right)\frac{\Omega}{\omega_{SL}}\frac{\Omega^2}{\omega_1^2} + \cdots \\ 2\frac{\Omega}{\omega_{SL}}\frac{\Omega}{\omega_1} + \left(\frac{\pi}{4}-1\right)\frac{\Omega^2}{\omega_1^2} + \cdots \\ \mp\frac{\Omega}{\omega_{SL}} + \left(2+\frac{\pi}{2}\right)\frac{\Omega^2}{\omega_1^2} \pm \frac{1}{6}\frac{\Omega^3}{\omega_{SL}^3} + \cdots \end{pmatrix}. \tag{20}$$

Only those terms with alternating signs are retained so that the only undesired terms are of third order and higher:

$$\begin{aligned} \frac{M_z}{M_x} &\approx \frac{\Omega}{\omega_{SL}} + \frac{1}{3}\frac{\Omega^3}{\omega_{SL}^3} - \frac{2\Omega}{\omega_{SL}}\frac{\Omega^2}{\omega_1^2} + \frac{1}{3}\frac{\Omega^3}{\omega_1^3} + \cdots \\ \frac{M_y}{M_x} &\approx \left(\frac{\pi}{4}-1\right)\frac{\Omega}{\omega_{SL}}\frac{\Omega^2}{\omega_1^2} + \left(\frac{17}{6}+\frac{\pi}{4}\right)\frac{\Omega^3}{\omega_1^3} + \cdots \end{aligned} \tag{21}$$

The major improvement in this scheme originates from the removal of the component proportional to Ω/ω_1 and orthogonal to the effective field.

Figures 2, 3 compare the alignment schemes of Eqs. (14), (19) for both ^{1}H and ^{15}N magnetization, respectively, using spin-lock field strengths and offsets that are appropriate for each class of spin. Each curve in the figures shows the angular deviation of magnetization from the spin-lock field calculated using Eq. (2) to describe each pulse, while evolution of magnetization during delays was given by z-rotations with angular frequency Ω; relaxation was neglected. It is quite clear that the ''refocused'' alignment scheme significantly outperforms the simple two-pulse method.

The results from the computations have been confirmed experimentally by measuring each of the magnetization components following alignment in a series of ^{1}H–^{15}N correlation maps. A standard ^{1}H–^{15}N HSQC pulse scheme was employed with the alignment schemes of Eqs. (14), (19) inserted after the first INEPT magnetization transfer (^{1}H to ^{15}N), where the term of interest is $2\mathbf{I}_z\mathbf{N}_z$. Subsequently only one of the three orthogonal components is returned to ^{1}H for detection. As can be seen in Fig. 3 there is an excellent correlation between theory and experiment.

Removing artifacts to higher order

The goal of the alignment schemes described above is to create pairs of orthogonal magnetization components in the ratio Ω/ω_{SL} so that magnetization from each spin can be placed along its effective field prior to the application of the spin-lock. Thus, for an x-spin lock we require that $M_z/M_x = \Omega/\omega_{SL}$, $M_y = 0$ so that $M_x = 1/\sqrt{1+(\Omega/\omega_{SL})^2}$, $M_z = (\Omega/\omega_{SL})/\sqrt{1+(\Omega/\omega_{SL})^2}$, assuming that the magnetization is normalized ($\|\vec{M}\| = 1$). In practice alignment is achieved through a chemical shift evolution period (χ in the sequences above) that can be thought of as an interval during which magnetization is transferred between orthogonal components, so that their ratio becomes $\tan(\Omega/\omega_{SL})$. The efficiency of the approach is predicated, therefore, on a linear buildup or transfer, $\tan(\Omega/\omega_{SL}) \approx \Omega/\omega_{SL}$. For nuclei with $|\Omega| > 0.4\omega_{SL}$ the transfer of magnetization from the ''starting'' component to the second orthogonal component [M_x to M_y in the schemes of Eqs. (14), (19)] becomes ''too efficient'', so that the linear approximation, $\tan(\Omega/\omega_{SL}) \approx \Omega/\omega_{SL}$, is violated leading ultimately to $M_z/M_x > \Omega/\omega_{SL}$, Eqs. (18), (21). It is straightforward to show that a linear magnetization transfer occurs initially, but that as the transfer proceeds and the orthogonal component builds up, the linear approximation becomes progressively less valid. Clearly the situation is worse for large values of Ω because the build-up occurs more rapidly. One approach for maintaining linearity would be to decrease the transfer time in a manner that relates to offset so that χ would effectively be shorter for spins with larger Ω. Alternatively, for a constant transfer period one could ''remove'' a portion of the transferred magnetization in an offset dependent manner at, say, the midpoint of the transfer period and store this component along the z-axis. At the end of the χ interval the stored magnetization would be combined with the component transferred during the second half of the period to generate the appropriate magnetization components for spin locking. This is the approach taken here.

The basic idea is illustrated in Fig. 4 where we focus on the fate of M_x (i.e., the component that is not transferred) during a ''modified'' $90^\circ_{\pm y}$ $-\chi$ -90°_x scheme. Let us suppose that for each offset Ω there are two fractions of spins with populations that depend on Ω. One fraction evolves uninterrupted during the χ period (trajectory denoted by the red line for $\Omega/2\pi = \omega_{SL}/2\pi = 1$ kHz), while the second fraction is acted upon by a 90° x-pulse at the midpoint of the χ interval. The fraction of spins in each pool must be chosen so that at the end of the χ period $M_x(t = 1/\omega_{SL}) = 1/\sqrt{1+(\Omega/\omega_{SL})^2}$ where M_x is the sum of x-components of magnetization from the blue

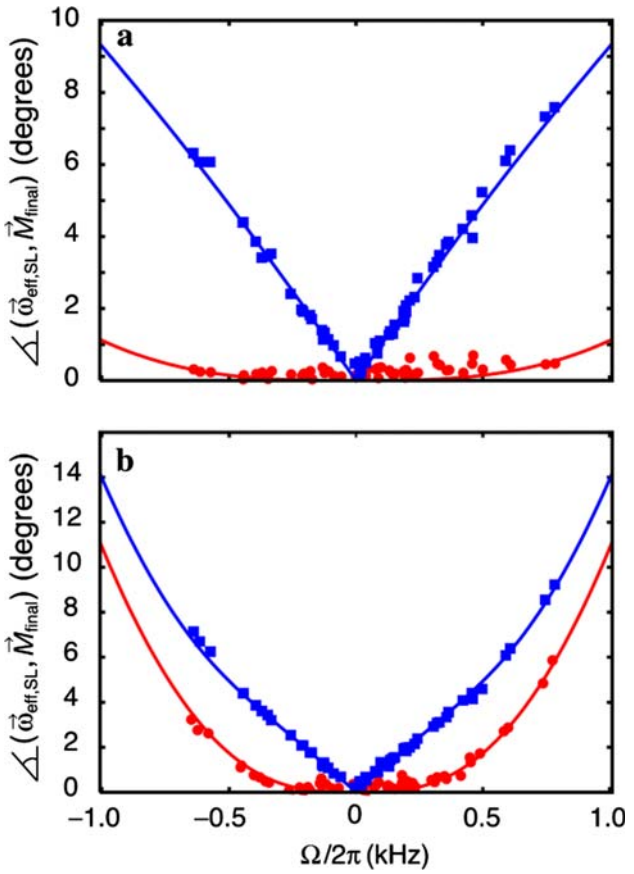

Fig. 3 Alignment of ^{15}N magnetization (details as in Fig. 2) using $90°_{\pm y} - \chi - 90°_{x}$ (blue) and $90°_{\pm y} - \chi - 90°_{x} - 180°_{\pm y} - \zeta$, (red) schemes. The field strength used for high power pulses is $\omega_1/2\pi$ = 6.25 kHz, with $\omega_{SL}/2\pi$ = 2.0 kHz (**a**) and 1 kHz (**b**). Calculations are shown with continuous lines, while experimental data are indicated with circles and squares. Experimental data were acquired using a 1 mM sample of the WT Fyn SH3 domain, 50 mM sodium phosphate, 0.2 mM EDTA, 0.05% NaN_3, 5% D_2O, pH 7, 25 °C, prepared as described previously (Maxwell and Davidson 1998; Di Nardo et al. 2004). Spectra were recorded at 600 MHz (^{1}H frequency)

and red pools of spins. Clearly it is not possible to execute the experiment as described. But it is possible to apply an x-pulse with an offset dependent flip angle $\Omega\delta/\omega_{SL}$ to all the spins, where δ is a factor that is chosen as described below. In this case the trajectory of M_x as a function of t ($0 \le t \le 1/\omega_{SL}$) is given by the green solid line (sum of the blue and red lines) and the value of M_x is equal to $1/\sqrt{1+(\Omega/\omega_{SL})^2}$ at the completion of the χ period. Of note, the green dashed line shows the trajectory of M_x during the ''simple'' $90°_{\pm y} - \chi - 90°_{x}$ scheme where it is clear that $M_x(1/\omega_{SL}) < 1/\sqrt{1+(\Omega/\omega_{SL})^2}$ (i.e. magnetization has been transferred from M_x too rapidly, depleting M_x beyond that optimal for the spin-lock).

Figure 5 illustrates the pulse scheme that has been developed with these considerations in mind. It is

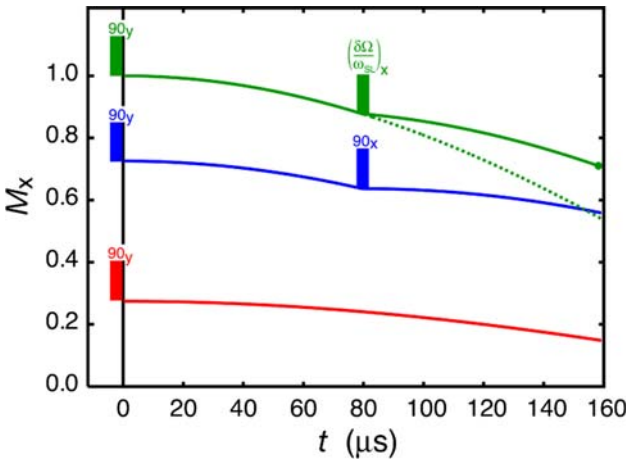

Fig. 4 Trajectory showing the depletion of x-magnetization during the χ element, for $0 \le t \le 1/\omega_{SL}$, $\omega_{SL}/2\pi = \Omega/2\pi$ = 1 kHz. The total magnetization is divided into two pools, red (27%) and blue (73%). The magnetization in the red pool follows a trajectory identical to that during the $90°_y$ –χ –$90°_x$ sequence, while the application of a 90_x pulse in the middle of the χ period effectively reduces the depletion of the x-magnetization in the blue pool. In practice, the magnetization is divided into the two pools by applying a rotation proportional to Ω/ω_{SL} around the x-axis at the half-point in the χ delay, as shown by the green trajectory that includes the total magnetization (red + blue). Optimal alignment is achieved at the end of the sequence, i.e, $M_x = 1/\sqrt{1+\Omega^2/\omega_{SL}^2} = 0.71$. As detailed in the text, the component of the magnetization that is orthogonal to M_x, $\vec{M} - M_x\hat{x}$ with $\left\|\vec{M} - M_x\hat{x}\right\| = 0.71$, must be placed along the z-axis prior to the spin-lock ($\|\vec{a}\| = \sqrt{\vec{a}\cdot\vec{a}}$)

worth noting at the outset that all of the delays in the sequence have been compensated to first order for off-resonance effects of the pulses (via the terms proportional to $1/\omega_1$) using the rules established above. Before presenting a detailed analysis of the scheme we provide a brief description so that a qualitative ''feel'' for the sequence can be obtained. The initial 90° x-pulse at point A creates $-y$ magnetization, with ''transfer to x via chemical shift evolution'' occurring during the interval between A and D. At the midpoint of this interval, between points B and C, a y-rotation element is inserted that rotates in an offset dependent manner a portion of the magnetization that has been transferred ($-M_y$ to M_x) to the z-axis where it is stored

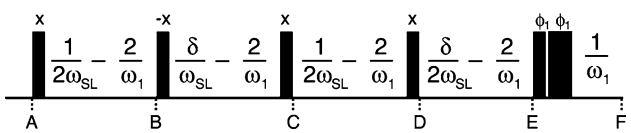

Fig. 5 Pulse scheme for improved alignment of magnetization along the effective magnetic field, $\vec{\omega}_{eff,SL} = \omega_{SL}\hat{x} + \Omega\hat{z}$. The factor δ is determined as described below. Narrow (wide) bars indicate 90° (180°) pulses. The phase cycle is $\phi_1 = (y, -y)$ together with inversion of the receiver

for the duration of the transfer period. This effectively decreases the rate of transfer (i.e., Ω) of magnetization between orthogonal components as averaged over the whole transfer period, χ, with the transfer among spins with larger offsets affected more significantly. Following the transfer period the pulse at point D rotates $-y$ magnetization to the z-axis, while the magnetization that has been stored along the z-axis (i.e., transferred during A to B) is returned to the transverse plane where it is orthogonal to the magnetization transferred during points C to D. At this point all the transferred magnetization resides in the x–y plane and during the ensuing delay between points D and E it is refocused along the x-axis. Finally, the subsequent pulses between E and F ensure that x and z-magnetization components are in the appropriate ratio so that net magnetization resides along the effective field.

In a more detailed manner, initially at point A the density operator is proportional to $\mathbf{I}_z$ and at point B it is given by

$$\boldsymbol{\sigma}_{\mathrm{B}} = \mathbf{I}_x \sin(\Omega/2\omega_{\mathrm{SL}}) - \mathbf{I}_y \cos(\Omega/2\omega_{\mathrm{SL}}). \tag{22}$$

The y-rotation element inserted between points B and C rotates $\mathbf{I}_x$ to $\mathbf{I}_z$, in a manner which depends on offset, Ω; as the offset of magnetization from the carrier increases and hence the "linear transfer" approximation described above becomes worse, an increasing amount of the transferred component is stored along the z-axis

$$\begin{aligned}\boldsymbol{\sigma}_{\mathrm{C}} = &+ \mathbf{I}_x \sin(\Omega/2\omega_{\mathrm{SL}})\cos(\Omega\delta/\omega_{\mathrm{SL}}) - \mathbf{I}_y \cos(\Omega/2\omega_{\mathrm{SL}}) \\ &+ \mathbf{I}_z \sin(\Omega/2\omega_{\mathrm{SL}})\sin(\Omega\delta/\omega_{\mathrm{SL}}).\end{aligned} \tag{23}$$

The scaling factor, δ, is determined as described below so as to optimize the alignment for nuclei within a specified frequency range from the carrier. The second interval of the $1/\omega_{\mathrm{SL}}$ evolution delay is between points C and D

$$\begin{aligned}\boldsymbol{\sigma}_{\mathrm{D}} = &+ \mathbf{I}_x \sin(\Omega/2\omega_{\mathrm{SL}})\cos(\Omega/2\omega_{\mathrm{SL}})[1+\cos(\Omega\delta/\omega_{\mathrm{SL}})] \\ &- \mathbf{I}_y \sin(\Omega/2\omega_{\mathrm{SL}})\sin(\Omega\delta/\omega_{\mathrm{SL}}) \\ &- \mathbf{I}_z[\cos^2(\Omega/2\omega_{\mathrm{SL}}) - \sin^2(\Omega/2\omega_{\mathrm{SL}})\cos(\Omega\delta/\omega_{\mathrm{SL}})],\end{aligned} \tag{24}$$

where

$$\frac{\langle\boldsymbol{\sigma}_{\mathrm{D}}|\mathbf{I}_y\rangle}{\langle\boldsymbol{\sigma}_{\mathrm{D}}|\mathbf{I}_x\rangle} = -\frac{\tan(\Omega\delta/2\omega_{\mathrm{SL}})}{\cos(\Omega/2\omega_{\mathrm{SL}})} \approx \tan(-\Omega\delta/2\omega_{\mathrm{SL}}). \tag{25}$$

Thus, at point D the transverse coherence, that comprises essentially all of the transferred magnetization, forms an angle of approximately $-\Omega\delta/2\omega_{\mathrm{SL}}$ with the x-axis and the delay between points D and E serves to refocus this magnetization so that it aligns along the x-axis. The $90°_{\phi 1}$-pulse brings the z-component of magnetization along $\hat{x}$, the x-component along $\hat{z}$, and the $180°_{\phi 1} - 1/\omega_1$ element refocuses the evolution that occurs during the $90°_{\phi 1}$ pulse. The small remaining y-component of magnetization is eliminated by the phase cycle so that

$$\begin{aligned}\boldsymbol{\sigma}_{\mathrm{F}} = &+ \mathbf{I}_x[\cos^2(\Omega/2\omega_{\mathrm{SL}}) - \sin^2(\Omega/2\omega_{\mathrm{SL}})\cos(\Omega\delta/\omega_{\mathrm{SL}})] \\ &+ \mathbf{I}_z\{\sin(\Omega/2\omega_{\mathrm{SL}})\cos(\Omega/2\omega_{\mathrm{SL}})[1+\cos(\Omega\delta/\omega_{\mathrm{SL}})] \\ &\times\cos(\Omega\delta/2\omega_{\mathrm{SL}}) + \sin(\Omega/2\omega_{\mathrm{SL}})\sin(\Omega\delta/\omega_{\mathrm{SL}}) \\ &\times\sin(\Omega\delta/2\omega_{\mathrm{SL}})\}.\end{aligned} \tag{26}$$

It remains to determine the length of the delay $\delta/\omega_{\mathrm{SL}}$ between point B and C in the sequence of Fig. 5 so as to obtain optimal alignment. In particular, the factor δ is chosen for optimal alignment of nuclei in the range of frequencies from the RF carrier given by $\Omega \in [-\alpha\omega_{\mathrm{SL}}, \alpha\omega_{\mathrm{SL}}]$. The components of the density operator at point F that are parallel and orthogonal to $\vec{\omega}_{\mathrm{eff,SL}}$ are defined as

$$\boldsymbol{\sigma}_{\mathrm{eff},\|} = \frac{\langle\boldsymbol{\sigma}_{\mathrm{F}}|\mathbf{I}_x\omega_{\mathrm{SL}} + \mathbf{I}_z\Omega\rangle}{\langle\mathbf{I}_x\omega_{\mathrm{SL}} + \mathbf{I}_z\Omega|\mathbf{I}_x\omega_{\mathrm{SL}} + \mathbf{I}_z\Omega\rangle}(\mathbf{I}_x\omega_{\mathrm{SL}} + \mathbf{I}_z\Omega) \tag{27}$$

and

$$\boldsymbol{\sigma}_{\mathrm{eff},\perp} = \boldsymbol{\sigma}_{\mathrm{F}} - \boldsymbol{\sigma}_{\mathrm{eff},\|} \tag{28}$$

respectively, and the factor δ that results in the optimal alignment, δ_{opt}, is the one that minimizes

$$\chi^2(\delta) = \int_{-\alpha\omega_{\mathrm{SL}}}^{\alpha\omega_{\mathrm{SL}}} \mathrm{d}\Omega \left\|\boldsymbol{\sigma}_{\mathrm{eff},\perp}\right\|^2. \tag{29}$$

It is noted that δ_{opt} is solely a function of α, and in particular δ_{opt} is independent of ω_{SL} since the density operators $\boldsymbol{\sigma}_{\mathrm{F}}$ and $\boldsymbol{\sigma}_{\mathrm{eff},\perp}$ are given entirely in terms of $\Omega/\omega_{\mathrm{SL}}$. The δ_{opt} is shown in Fig. 6 for different values of the scaling factor α.

Figure 7 shows the alignment obtained with the improved scheme in Fig. 5 for spin-lock fields of 500 and 250 Hz, with the alignment optimized for different frequency ranges. Alignment of the magnetization within 1° from the effective field can be obtained for all nuclei in the frequency range $[-\omega_{\mathrm{SL}}, \omega_{\mathrm{SL}}]$, using $\delta = 1.35$. Alternatively, the spins can be aligned within five degrees from the effective field when the sequence

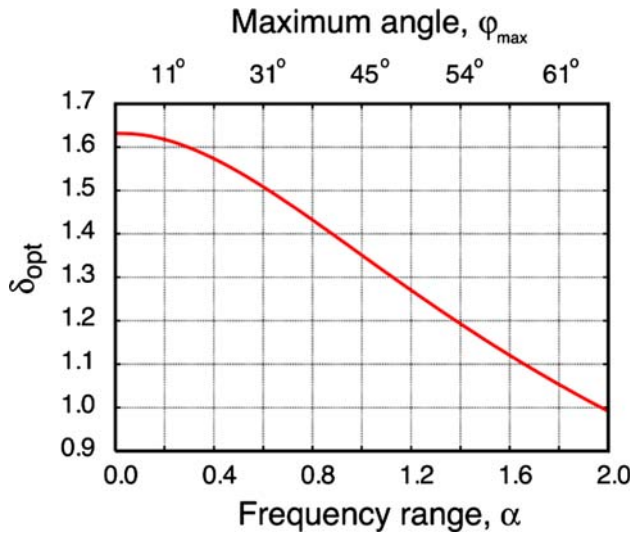

Fig. 6 The factor δ_{opt} for optimal alignment of magnetization over the range of frequencies $[-\alpha\omega_{SL}, \alpha\omega_{SL}]$, along with the angle, φ_{max}, between $\vec{\omega}_{SL}$ (x-axis in the discussion above) and magnetization from spins with offset $\alpha\omega_{SL}$ from the carrier. The δ_{opt} is that δ producing a global minimum for $\chi^2(\delta)$ in Eq. (29)

is optimized over the larger frequency range, $[-2\omega_{SL}, 2\omega_{SL}]$.

As a final note Fig. 8 compares the performance of an adiabatic pulse (red; 1 kHz maximum field, 25 kHz sweep from $\Omega/2\pi$ = +25 kHz to 0 kHz for a duration of 4 ms) and the pulse/delay scheme of Fig. 5 (blue; ω_{SL} = 1 kHz, α = 1, duration of 481 μs) for an ''on-resonance'' spin-lock. It is worth noting that although the adiabatic pulse ensures that $M_z/M_x \approx \Omega/\omega_{SL}$ over a wider bandwidth (a), the angle between the magnetization and the spin-lock field (which is the important criterion for evaluating performance) is smaller over a frequency range of $\pm\omega_{SL}$ for the pulse/delay sequence (b).

Concluding remarks

A formalism has been presented that enables an ''intuitive'' understanding of the evolution of magnetization due to off-resonance pulses. Building on this intuition improved schemes relative to the standard 90°-delay-90° element for magnetization alignment have been constructed. It remains clear that for applications involving very large off-resonance spin-locks, such as would be the case in off-resonance $R_{1\rho}$ measurements, alignment via adiabatic schemes is preferred. However, for on-resonance studies the sequence of Fig. 5 generates alignment that is very competitive with what can be achieved using adiabatic pulses and on a time-scale that is approximately an order of magnitude shorter. This could have important implications in studies where relaxation losses are an issue or where evolution during the course of the lengthy adiabatic pulses must be taken into account (Korzhnev et al. 2003).

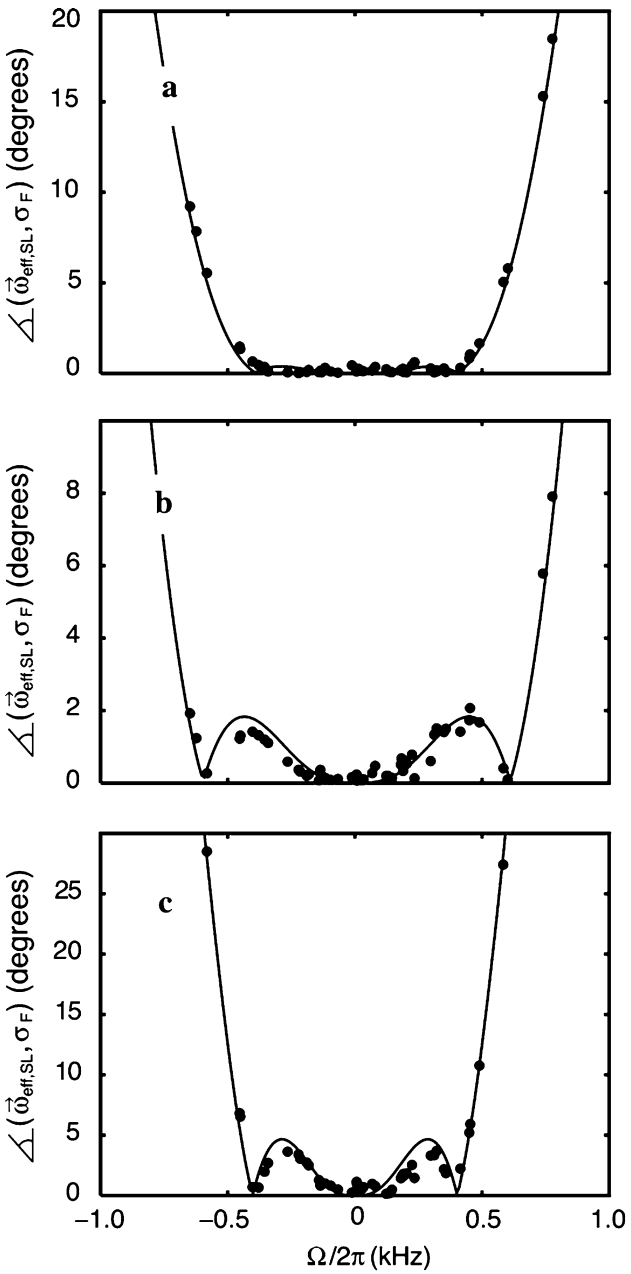

Fig. 7 Alignment of ^{15}N magnetization along the effective magnetic field, $\vec{\omega}_{eff,SL}$, calculated as the angle between $\vec{\omega}_{eff,SL}$ and the magnetization that is produced immediately following the alignment scheme of Fig. 5. Calculated and experimental data are shown with continuous lines and circles, respectively. (**a**) $\omega_{SL}/2\pi$ = 500 Hz, with δ optimized for the range [–500 Hz, 500 Hz], i.e., α = 1.0 and δ_{opt} = 1.35. (**b**) $\omega_{SL}/2\pi$ = 500 Hz, δ optimized for [–750 Hz, 750 Hz], i.e. α = 1.5 and δ_{opt} = 1.16. (**c**) $\omega_{SL}/2\pi$ = 250 Hz with δ optimal for the range [–500 Hz, 500 Hz], i.e., α = 2.0 and δ_{opt} = 1.0

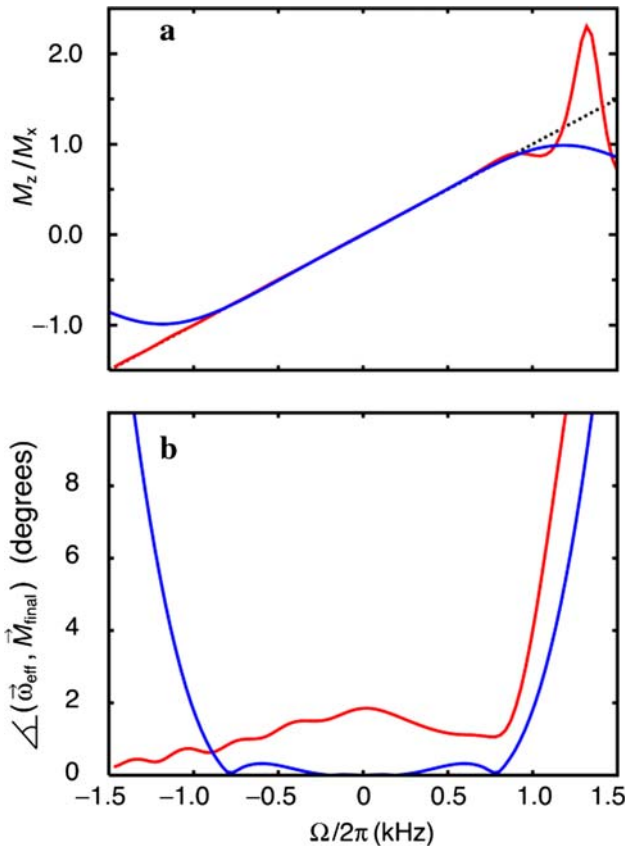

Fig. 8 Simulations of alignment of magnetization with the scheme of Fig. 5 (blue) or by an adiabatic sweep (red). Values of $\omega_1/2\pi = 6.25$ kHz, $\omega_{SL}/2\pi = 1$ kHz and $\alpha = 1$ were assumed. The adiabatic pulse had a $\tan(t)/\tanh(t)$ profile (Mulder et al. 1998) with a 4 ms sweep from +25 to 0 kHz in time steps of 20 μs and a maximum amplitude of 1 kHz. (**a**) M_z/M_x ratio obtained for the two alignment sequences along with the ratio that corresponds to ideal alignment in the x–z plane (dotted line). (**b**) The angle between the spin-lock field, $\vec{\omega}_{eff,SL} = \omega_{SL}\hat{x} + \Omega\hat{z}$, and the magnetization following alignment as a function of offset. For the adiabatic sweep the residual M_y component is the primary contributor to misalignment when $\Omega/2\pi < 800$ Hz, while for $\Omega/2\pi > 800$ Hz both M_y and the component orthogonal to $\vec{\omega}_{eff,SL}$ in the x–z plane contribute. The M_y component is eliminated by the $\pm y$ phase cycle in the sequence of Fig. 5; in this scheme the misalignment is due to the component orthogonal to $\vec{\omega}_{eff,SL}$ in the x–z plane

Acknowledgements This work was supported by a grant from the Natural Sciences and Engineering Research Council of Canada. DFH thanks the Danish Agency for Science, Technology and Innovation (J.no. 272-05-0232) for a postdoctoral fellowship. LEK holds a Canada Research Chair in Biochemistry. We thank Arash Zarrine-Afsar for preparation of the WT Fyn SH3 domain sample used in this work.

References

Akke M, Palmer AG (1996) Monitoring macromolecular motions on microsecond to millisecond time scales by R1rho-R1 constant relaxation time NMR spectroscopy. J Am Chem Soc 118:911–912

Allerhand A, Doddrell D, Glushko U, Cochran DW, Wenkert E, Lawson PJ, Gurd FRN (1971) Carbon-13 Fourier tranform nuclear magnetic resonance 3. Conformation and segmental motion of native and denatured ribonuclease-a in solution – application of natural-abundance carbon-13 partially relaxed Fourier transform nuclear magnetic resonance. J Am Chem Soc 93:544–546

Dayie KT, Wagner G, Lefevre JF (1996) Theory and practice of nuclear spin relaxation in proteins. Annu Rev Phys Chem 47:243–282

Deverell C, Morgan RE, Strange JH (1970) Studies of chemical exchange by nuclear magnetic relaxation in rotating frame. Mol Phys 18:553–559

Di Nardo AA, Korzhnev DM, Stogios PJ, Zarrine-Afsar A, Kay LE, Davidson AR (2004) Dramatic acceleration of protein folding by stabilization of a nonnative backbone conformation. Proc Natl Acad Sci USA 101:7954–7959

Ernst RR, Bodenhausen G, Wokaun A (1987) Principles of nuclear magnetic resonance in one and two dimensions. Oxford University Press, Oxford

Griesinger C, Ernst RR (1987) Frequency offset effects and their elimination in NMR rotating-frame cross-relaxation spectroscopy. J Magn Reson 75:261–271

Gust D, Moon RB, Roberts JD (1975) Applications of natural-abundance nitrogen-15 nuclear magnetic resonance to large biochemically important molecules. Proc Natl Acad Sci USA 72:4696–4700

Henry GD, Weiner JH, Sykes BD (1986) Backbone dynamics of a model membraneprotein – C13 NMR-spectroscopy of alanine methyl-groups in detergent-solubilized m13 coat protein. Biochemistry 25:590–598

Ishima R, Torchia DA (2000) Protein dynamics from NMR. Nat Struct Biol 7:740–743

Kay LE, Marion D, Bax A (1989a) Practical aspects of 3d heteronuclear NMR of proteins. J Magn Reson 84:72–84

Kay LE, Torchia DA, Bax A (1989b) Backbone dynamics of proteins as studied by N15 inverse detected heteronuclear NMR-spectroscopy – application to staphylococcal nuclease. Biochemistry 28:8972–8979

Korzhnev DM, Orekhov VY, Dahlquist FW, Kay LE (2003) Off-resonance R1rho relaxation outside of the fast exchange limit: An experimental study of a cavity mutant of T4 lysozyme. J Biomol NMR 26:39–48

Marion D, Bax A (1988) P-cosy, a sensitive alternative for double-quantum-filtered cosy. J Magn Reson 80:528–533

Maxwell KL, Davidson AR (1998) Mutagenesis of a buried polar interaction in an SH3 domain: Sequence conservation provides the best prediction of stability effects. Biochemistry 37:16172–16182

Mulder FAA, De Graaf RA, Kaptein R, Boelens R (1998) An off-resonance rotating frame relaxation experiment for the investigation of macromolecular dynamics using adiabatic rotations. J Magn Reson 131:351–357

Nirmala NR, Wagner G (1988) Measurement of C13 relaxation-times in proteins by two-dimensional heteronuclear H1-C13 correlation spectroscopy. J Am Chem Soc 110:7557–7558

Palmer AG, Massi F (2006) Characterization of the dynamics of biomacromolecules using rotating-frame spin relaxation NMR spectroscopy. Chem Rev 106:1700–1719

Palmer AG, Williams J, McDermott A (1996) Nuclear magnetic resonance studies of biopolymer dynamics. J Phys Chem 100:13293–13310

Peng JW, Wagner G (1992) Mapping of spectral density-functions using heteronuclear nmr relaxation measurements. J Magn Reson 98:308–332

Richarz R, Nagayama K, Wuthrich K (1980) C13 nuclear magnetic-resonance relaxation studies of internal mobility of the polypeptide-chain in basic pancreatic trypsin-inhibitor and a selectively reduced analog. Biochemistry 19:5189–5196

Sørensen OW, Eich GW, Levitt MH, Bodenhausen G, Ernst RR (1983) Product operator-formalism for the description of NMR pulse experiments. Prog Nucl Magn Reson Spectrosc 16:163–192

Yamazaki T, Muhandiram R, Kay LE (1994) NMR experiments for the measurement of carbon relaxation properties in highly enriched, uniformly C13,N15-labeled proteins – application to C13(alpha) carbons. J Am Chem Soc 116:8266–8278